New Journal of Physics
The open access journal at the forefront of physics

Deutsche Physikalische Gesellschaft DPG
IOP Institute of Physics

Published in partnership with: Deutsche Physikalische Gesellschaft and the Institute of Physics

OPEN ACCESS

RECEIVED
3 October 2021

REVISED
14 November 2021

ACCEPTED FOR PUBLICATION
19 November 2021

PUBLISHED
13 December 2021

PAPER

Lamb-dip cavity ring-down spectroscopy of acetylene at 1.4 μm

E Fasci, S Gravina, G Porzio, A Castrillo* and L Gianfrani

Dipartimento di Matematica e Fisica, Università della Campania 'Luigi Vanvitelli', Caserta, Italy
* Author to whom any correspondence should be addressed.

E-mail: antonio.castrillo@unicampania.it

Keywords: acetylene, COMB assisted FS-CRDS, Lamb-dip spectroscopy, frequency metrology, MARVEL

Abstract

Doppler-free saturated-absorption Lamb dips are observed for weak vibration-rotation transitions of C_2H_2 between 7167 and 7217 cm^{-1}, using a frequency-comb assisted cavity ring-down spectrometer based on the use of a pair of phase-locked diode lasers. We measured the absolute center frequency of sixteen lines belonging to the $2\nu_3 + \nu_5^1$ band, targeting *ortho* and *para* states of the molecule. Line pairs of the P and Q branches were selected so as to form a 'V'-scheme, sharing the lower energy level. Such a choice made it possible to determine the rotational energy separations of the excited vibrational state for J-values from 11 to 20. Line-center frequencies are determined with an overall uncertainty between 3 and 13 kHz. This is over three orders of magnitude more accurate than previous experimental studies in the spectral region around the wavelength of 1.4 μm. The retrieved energy separations provide a stringent test of the so-called MARVEL method recently applied to acetylene.

1. Introduction

In its electronic ground state, acetylene is a linear, centrosymmetric, nonpolar molecule whose spectral features are important in a large variety of research fields, including temperature metrology [1], combustion science [2], organic electronics [3], and biomedicine [4]. So far, most of the spectroscopic studies have been motivated by astrophysical and planetary science applications of acetylene's line parameters. In fact, acetylene is expected to be present in the exoplanetary atmospheres [5, 6]. Theoretical atmospheric models, supported by chemical laboratory data, predict a relatively large volume mixing-ratio for acetylene in the atmosphere of young Earth-like exoplanets [7]. Clear C_2H_2 signatures can be found in star forming regions [8], as well as in brown dwarf disks [9]. The astrophysical importance of C_2H_2 has been recently highlighted by Tennyson's group [10], who has computed a new ro-vibrational line list for the ground electronic state of the main isotopologue of acetylene. Such a line list is extremely useful to characterize the atmospheres of exoplanets and cool stars [10]. However, Tennyson and coworkers advise that more work needs to be done to achieve the precision required for studies of exoplanets using high-resolution spectroscopy. In this respect, the MARVEL analysis of Chubb *et al* [11] can be exploited, especially if it is corroborated by new laboratory data in the sub-Doppler regime and assisted by the technology of optical frequency comb synthesizers. Relatively strong acetylene lines in the near-infrared can be saturated by using cavity-based spectroscopy techniques. This experimental strategy has been recently implemented to perform Lamb-dip frequency measurements on the $\nu_1 + \nu_3$ band near 1.5 μm [12, 13]. Similarly, much weaker lines of the $\nu_1 + 3\nu_3$ band at 0.789 μm have been saturated [14].

The 1.4 μm spectral region is rich of C_2H_2 vibrational transitions. Characterized by a variation of the polyad number equal to 11, these bands have been extensively studied by using high-resolution Fourier-transform infrared spectroscopy [15, 16]. Recently, Lyulin and Perevalov collected the parameters for a huge number of lines of the main C_2H_2 isotopologue, covering the 3–10 000 cm^{-1} spectral range, in the temperature interval between 296 and 1000 K [17].

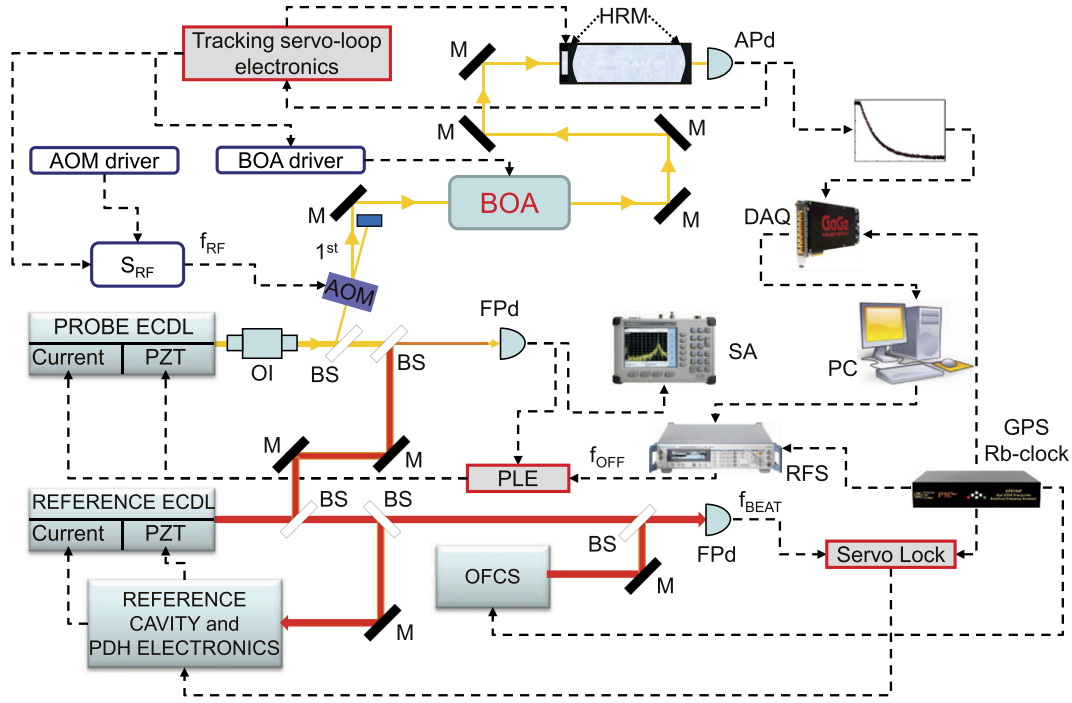

Figure 1. Schematic diagram of the CC-FS-CRDS. OI stands for optical isolator; OFCS, Rb-clock disciplined optical frequency comb synthesizer; BS, beam splitter; M, mirror; HRM, high-reflectivity mirrors; FPd, fast photodiode; PLE, phase-locking electronics; AOM, acoustic-optic modulator; BOA, booster optical amplifier; S_{RF}, radio-frequency switches; APd, avalanche photodetector; DAQ, data acquisition board; SA, spectrum analyzer; RFS, radio-frequency synthesizer; PC, personal computer.

In this paper, we report on the outcomes of a refined study on the $2\nu_3 + \nu_5^1$ band, as performed by means of frequency-stabilized, comb-calibrated, cavity ring-down spectroscopy near 1.4 μm. Doppler-free saturated-absorption Lamb dips were observed for sixteen vibration-rotation lines between 7167 and 7217 cm^{-1}, targeting *ortho* and *para* states of acetylene. Line pairs of the P and Q branches were selected so as to form a V-scheme, sharing the lower energy level. By measuring the line center frequencies, it was possible to determine the rotational energy separations of the excited vibrational state for J-values from 11 to 20. The spectrometer is an upgraded version of that developed for precision spectroscopy of HD and described in [18], the main novelty being the use of a BOA—Booster Optical Amplifier, to increase the optical power injected into the high-finesse cavity.

2. Methods and data analysis

In this section, the experimental setup is described, also providing a detailed explanation of the frequency calibration method, along with data acquisition and spectral analysis procedures.

2.1. Experimental apparatus

Absorption spectra were acquired using an updated version of the comb-calibrated frequency-stabilized cavity ring-down spectrometer (CC-FS-CRDS), whose first implementation is discussed in references [18, 19]. The experimental setup, depicted in figure 1, consists of four modules. The first of them is an optical frequency comb synthesizer (OFCS, from Menlo Systems, model FC1500-250), traceable to a 10-MHz GPS-disciplined time base signal provided by a Rb-clock (Precision Test Systems, model GPS10eR). This latter has an accuracy of a few parts in 10^{-14} and a 1 s Allan deviation of 2.5×10^{-12}. The second one is an external-cavity diode laser (ECDL), emitting at 1.4 μm, tightly locked to a high-finesse cavity by means of the Pound–Drever–Hall (PDH) technique so as to narrow its emission line width from about 1 MHz down to 7 kHz for an observation time of 1 ms [20]. This laser acts as a reference laser (RL) for the experiment, being the PDH cavity locked at $f_{BEAT} = 20$ MHz from one of the comb teeth. The third module is a second ECDL, namely the probe laser (PL), which is used for the interrogation of the C_2H_2 gas samples. It is phase-locked to the RL following the scheme already described in reference [21]. The fourth part of the setup is a high-finesse ring-down (HFRD) optical cavity equipped with a tracking servo-loop circuit so that it could follow the PL while its frequency is scanned across a selected transition.

In detail, the HFRD cavity consists of two plano-concave mirrors with a radius of curvature of 1 m (from Layertec GmbH) and a nominal reflectivity greater than 99.99%, mounted on a Zerodur block, with a

cylindrical hole around its axis. A piezoelectric transducer (PZT) is mounted on one of the two mirrors, allowing for a fine tuning of the cavity length. This latter is 43 cm, thus leading to a free-spectral-range (FSR) of 348.5 MHz. The cavity is equipped with an absolute pressure gauge having an accuracy of 2% and a calibrated 100 Ω Pt-resistance thermometer. From cavity ring-down events acquired under vacuum conditions, we infer a finesse, F, of about 120 000, while the cavity-mode width is 2.9 kHz. At the output of the cavity, an InGaAs avalanche detector (APd, from Thorlabs, model APD110C, with an effective bandwidth of 420 kHz, a conversion gain of 0.9×10^6 V/W, and a noise-equivalent power of 0.46 pW $\mathrm{Hz}^{-1/2}$) is used to observe the ring-down events. The DC-coupled detector signal is digitized by means of an acquisition board (Gage, model CSE1622), having a sample rate of 10^7 samples/s and a vertical resolution of 16 bit, while its sampling clock is disciplined by the same 10 MHz signal used for the stabilization of the OFCS. For each ring-down event, 7000 points are recorded for a time span of 700 μs.

The light emitted by the PL is split in two parts. The first one is overlapped with a portion of the RL and sent to a 12 GHz photodetector (New Focus, model 1567-A) thus providing a beat note signal. The other one is coupled into the HFRD cavity, after passing into an acusto-optic modulator (AOM), a Booster Optical Amplifier (BOA, Thorlabs, model BOA1036P), and an optical fiber (not shown in figure 1) for spatial filtering.

The beat frequency, properly rescaled and compared to the signal of a radio-frequency (RF) synthesizer (Rohde & Schwarz, model SMC100A), is used as input of a servo loop which guarantees a tight phase-lock of the PL to the RL. The locking is implemented with a variable offset (f_{OFF}) that can be remotely controlled with the desired resolution in order to perform highly linear and accurate frequency scans of PL around an arbitrary center frequency [21, 22]. It is worth noting that also the RF synthesizer is disciplined by the Rb-clock.

Before entering the HFRD cavity, the PL light passes through a free-space AOM, which produces a first-order diffracted beam with a frequency shift, f_{RF}, of about 80 MHz. Cavity decay events are initiated by switching off the RF signal driving the AOM. This is accomplished by means of a pair of RF switches (RF BAY, model RFS-1) ensuring an extinction ratio of 90 dB. The first-order diffracted beam emerging from the AOM is amplified by the BOA up to about 20 mW. The BOA is controlled by a laser driver (ILX Lightwave, model LDC 3744B) and a 200 MHz bandwidth laser switch (IC-Haus, model IC-HG) following the scheme proposed in reference [23]. The use of the BOA is advantageous for a twofold reason: on the one hand, it increases the optical power incident on the HFRD cavity; on the other hand, it guarantees a further enhancement of the light extinction ratio. The output signal of the APd is used as input to a threshold detector, in order to monitor whether a resonance condition takes place while scanning the PL frequency. By properly setting the threshold signal (usually at 2 V), it is possible to detect only the occurrence of a TEM_{00} excitation. In this case, a 0–5 V TTL signal is produced and sent, as a trigger, to the data acquisition board. The same TTL pulse is simultaneously sent to the AOM switches and to the laser switch driving the BOA in order to suddenly switch off the laser beam. The threshold detector unit is part of the tracking servo-loop circuit, which was implemented so that the cavity could follow the PL frequency scans, thus allowing for high-resolution spectral acquisitions. This circuit is described in reference [19].

For the purpose of investigating the detection limit of the CC-FS-CRDS spectrometer, a ring-down Allan variance analysis is carried out under high-vacuum conditions. This latter is performed recording more than 450 000 ring-down events (over a time span of less then 1 h) at a fixed frequency of the PL. The mean value, τ_0, and the standard deviation, σ_{τ_0}, of the measured ring-down time distribution are 54.261 μs and 0.026 μs, respectively. This corresponds to a normalized reproducibility of 5×10^{-4} which gives a reliable estimate of the short-term reproducibility of the spectrometer. It is worth nothing that this result represents an improvement of a factor 10 as compared to reference [19]. On the other hand, the analysis reveals that the Allan deviation decreases following a $1/\sqrt{\tau}$ law, being τ the integration time, while it departs from this behavior when τ is greater than 15 s. At 1 s of integration time, the deviation is equal to 1.7×10^{-3} μs, while at $\tau = 10$ s (corresponding to 1500 ring-down events) it reaches a minimum value, $\sigma_{\tau_{\mathrm{min}}}$, of 8×10^{-4} μs. This latter translates into a minimum detectable absorption coefficient $\alpha_{\mathrm{min}} = \frac{\sigma_{\tau_{\mathrm{min}}}}{c\tau_0^2} = 9 \times 10^{-12}$ cm^{-1}, while the noise equivalent absorption (NEA) figure is $\frac{\sigma_{\tau_0}}{c\tau_0^2}\sqrt{\frac{2}{f_{\mathrm{rate}}}} = 3 \times 10^{-11}$ cm^{-1} $\mathrm{Hz}^{-1/2}$, being c the speed of light and f_{rate} the ring-down acquisition frequency (equal to 150 Hz in our experimental conditions).

2.2. Comb referencing and absolute frequency measurements

The PL is referenced to the OFCS so that each absorption spectrum is characterized by an absolute frequency axis. In particular, the frequency of the RL, f_{RL}, can be easily inferred form the equation:

$$f_{\mathrm{RL}} = N \times f_{\mathrm{REP}} \pm f_{\mathrm{CEO}} \pm f_{\mathrm{BEAT}}, \tag{1}$$

where N is the comb tooth order, $f_{REP} = 250$ MHz and $f_{CEO} = 20$ MHz are the comb repetition rate and carrier envelope offset frequency, respectively. The $\pm$ signs can be easily determined by slightly varying f_{CEO} and f_{REP} and observing the consequent variation of f_{BEAT}. On the other hand, the tooth order can be obtained by measuring the wavelength of the RL by means of a wavemeter (not shown in figure 1). This latter has an accuracy of 30 MHz, namely, smaller than half of the comb mode spacing. In our setup, N is found to be in the interval 859 468–865 438, depending on the molecular transition under investigation. Finally, the signs for f_{CEO} and f_{BEAT} are always positive. It must be noted that the in-loop relative stability of the RL frequency with respect to the OFCS is found to be 2×10^{-14} for an integration time of 1 s, as determined from a modified Allan deviation analysis [1]. However, this value does not include the frequency variations of the GPS Rb-clock to which the OFCS is referenced. This latter limits the RL frequency stability to 2.5×10^{-12}. On the other hand, it is important to highlight that the combined in-loop reproducibility of the carrier-envelope offset frequency and repetition rate is at the level of 3.4×10^{-13} that is smaller than the uncertainty associated to the Rb-clock stability.

Once the f_{RL} is unequivocally determined by means of equation (1), the frequency of the portion of the PL interacting with the gaseous sample, f_{PL}, can be easily measured according to the following equation:

$$\begin{aligned} f_{PL} &= f_{RL} + f_{RF} + f_{OFF} \\ &= N \times f_{REP} + f_{CEO} + f_{BEAT} + f_{RF} + f_{OFF}. \end{aligned} \tag{2}$$

The AOM driver is the only device that is not referenced to the Rb-clock. However, f_{RF} is routinely measured using a 12-digits universal counter (Agilent, model 53131A), which in turn is locked to the common time base of the experiment. On a day by day basis, f_{RF} is found to be stable within 1.8 Hz, the mean value being equal to 80 000 267.4 Hz, as determined over the whole measurement time span.

An arbitrarily large number of points for each absorption spectrum can be obtained with a fine step-by-step tuning of f_{OFF}. In the usual experimental conditions, frequency scans of 2.5 GHz are performed. This frequency range is wide enough to capture the Lamb-dip signature as well as the Doppler-broadened profile and the baseline signal.

To optimize the measurement time without loosing the required accuracy and resolution of the frequency axes around the line center, each PL scan is performed with an adaptive strategy, which consists in setting a variable frequency step depending on the portion of the scan. More particularly, a frequency step of 120 kHz was used for the 32 MHz wide portion around the line center, while the step increases up to 40 MHz elsewhere in the scan. Five ring-down events are acquired for each step, except for the high-resolution window, where twenty repeated acquisitions of the exponential decay are performed. As a consequence of this experimental strategy, an absorption spectrum is acquired in about 2 min. A LabView code was expressly developed to implement this strategy and perform the data acquisitions.

2.3. Spectral analysis

When the light transmitted through the cavity reaches the threshold, the PL light is switched off and the APd detector monitors the exponential decay. The absorption coefficient, α (in cm^{-1}), is derived using the well-known CRDS law:

$$\alpha(\nu) = \frac{1}{c}\left[\frac{1}{\tau(\nu)} - \frac{1}{\tau_0}\right], \tag{3}$$

where $\tau(\nu)$ is the decay time of the ring-down event at the PL frequency ν. $\tau(\nu)$ is retrieved from the time-dependent detector signal, S_{det}, which is modeled according to the equation:

$$S_{det}\ (t) = S_0 \times e^{-\frac{t}{\tau(\nu)}} + S_b, \tag{4}$$

where S_0 and S_b, the amplitude of the decay signal and a constant offset, respectively, are treated as free parameters along with $\tau(\nu)$.

For the P13e line at 7186.011420 cm^{-1}, the Einstein coefficient amounts to 0.030 23 $\frac{1}{s}$, while the line strength is 4.878×10^{-23} cm/molecule [24]. Using these values, we calculated a saturation intensity, I_{sat}, of about 1.7×10^7 W m^{-2} at a pressure of 1 Pa [25]. On the other hand, according to the formula given in reference [26] and considering a 0.1% mode-matching parameter (M), we can estimate that the intracavity power is of the order of 0.2 W, which translates into an intensity, I_{cav}, of 3.6×10^5 W m^{-2}, for a cavity beam waist of about 420 μm. From these experimental conditions, a saturation parameter $G = \frac{I_{cav}}{I_{sat}}$ of about 0.02 can be inferred. Such a value justifies the assumption of a weak saturation regime. In reason of that, we decided to use the simple model of equation (4), avoiding the implementation of a non-exponential model that would take saturation effects into account [27]. Similar circumstances apply to all the transitions that were investigated in the present work. It is worth noting that no evidence of non-exponential decays in the fit residuals is observed.

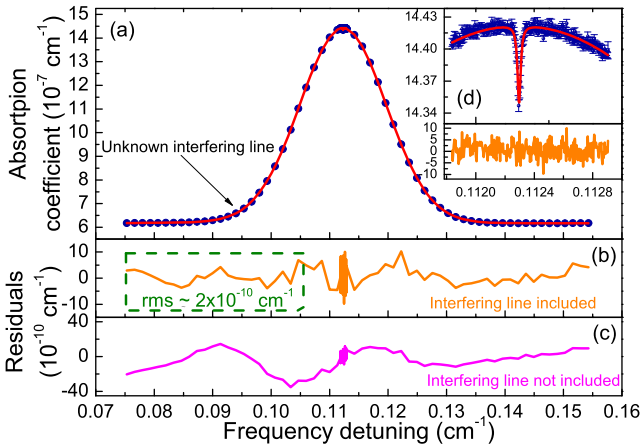

Figure 2. Panel (a): example of CRDS spectrum for the P13e line at a pressure of 0.25 Pa. The spectrum consists of 327 data points with variable frequency steps. Panel (b): example of residuals, as obtained from the application of the fitting procedure to the equation (5), after the inclusion of the interfering line. Panel (c): residuals without adding the interfering line. Panel (d): Lamb-dip spectrum along with the residuals of the fit using a Lorentzian function.

Each absorption spectrum is modeled using the following equation:

$$\alpha(\nu) = (P_0 + P_1\nu) + A_{\mathrm{D}} \times g_{\mathrm{D}}(\nu - \nu_{\mathrm{D0}}) - A_{\mathrm{L}} \times g_{\mathrm{L}}(\nu - \nu_{\mathrm{L0}}) \tag{5}$$

P_0 and P_1 being two baseline parameters that take into account possible variations due to a slightly dependence of the mirrors' reflectivity on ν, A_{D} the integrated absorption coefficient of the Doppler broadened profile, $g_{\mathrm{D}}(\nu - \nu_{\mathrm{D0}})$ a normalized Doppler lineshape function centered at ν_{D0}, A_{L} the amplitude of the Lamb-dip feature, and $g_{\mathrm{L}}(\nu - \nu_{\mathrm{L0}})$ a normalized Lorentzian lineshape function having its line center frequency at ν_{L0}.

An example spectrum is reported in panel (a) of figure 2. Fits residuals, resulting from the application of a Levenberg–Marquardt χ^2 minimization routine, are also shown. In the fitting procedure, the free parameters are A_{D}, A_{L}, ν_{D0}, ν_{L0}, P_0 and P_1, as well as the Doppler width, Γ_{D}, and Lorentzian width, Γ_{L}. It must be noted that, for some of the investigated transitions, fit residuals reveal the presence of a small interfering line otherwise not directly visible from the absorption spectrum alone. This is the case of the P13e transition, whose residuals are shown in panel (c) of figure 2. The presence of an interfering line is taken into account by adding a second Doppler-broadened line shape function to equation (5). Panel (b) of figure 2 shows that the inclusion of this line in the fitting procedure leads to a significant improvement of the residuals, thus reaching a deviation between theory and experiment comparable to the noise level. The root-mean-square value of the residuals amount to 2×10^{-10} cm^{-1}, which translates into a signal-to-noise ratio (SNR) of about 4000 (for the Doppler-broadened line). Similar values were found for all the investigated transitions. The inset of panel (d) of figure 2 shows the Lamb-dip along with the residuals of a fit to a Lorentzian profile. Also in this case, the level of agreement is comparable to the noise level.

3. Results and discussion

For each of the investigated transitions, the C_2H_2 gas pressure is varied in the range from 0.25 to 3.5 Pa, for a total of eleven values. In correspondence of each of them, ten consecutive spectra are recorded and individually fitted so as to determine the Lamb-dip center frequency (at a given pressure) as the mean of ten consecutive measurement's runs. As shown in figure 3, a weighted linear fit of the center frequency as a function of the pressure is performed in order to extrapolate the zero-pressure value. In the case of the P13e transition, the line center frequency is found to be 215 431 228 966(2) kHz, the fractional statistical uncertainty being 9×10^{-12}. It is worth noting that the pressure axis of figure 3 results from a 'spectroscopic' procedure. In other words, the C_2H_2 pressure is obtained from the integrated absorption coefficient, A_{D}, and the line intensity factors reported in [24]. Assuming that the isotopic abundance of the acetylene bottle is the natural one, the pressure, p, is retrieved using the equation $p = (\kappa A_{\mathrm{D}} k_{\mathrm{B}} T)/S$, where κ is a factor taking into account the gas purity (equal to 99.8%), S is the line intensity, T is the measured temperature, and k_{B} is the Boltzmann constant. The retrieved pressures are in very good agreement with those measured using the absolute pressure gauge, within the uncertainty coming from all the quantities involved in this determination.

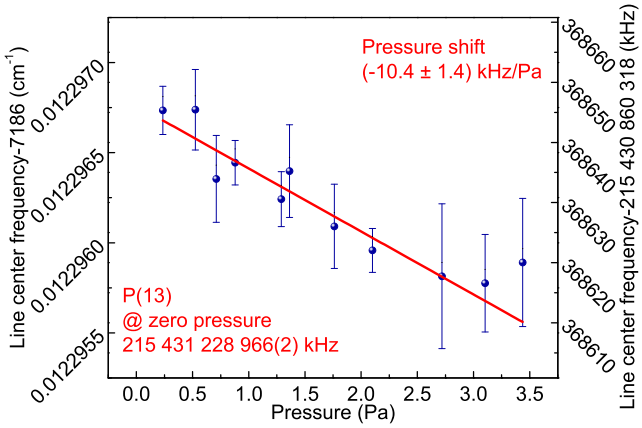

Figure 3. Center frequencies retrieved as function of the C_2H_2 pressure. The weighted best-fit line allows one to determine the zero-pressure center frequency.

The linear fit also provides the pressure shifting coefficient that is $-10.4(1.4)$ kHz Pa^{-1}. It must be noted that the pressure-induced shift reported in the Doppler regime for a line of the same vibrational band, namely the P14e transition at 7183.388 97 cm^{-1}, was $-1.996(4)$ kHz Pa^{-1} [21], which is far from the value reported in this paper. A similar mismatch has been already observed in a previous study on C_2H_2 [14], and also for other molecules such as CO [28, 29] and H_2O [30, 31].

The experimental procedure described above is applied to several lines of both P and Q branches, allowing for an accurate retrieval of their center frequencies.

The measured frequencies are reported in the second column of table 1. A comparison with different data sets is also provided. In particular, we compared our determinations with:

(a) Data included in the HITRAN database [24]. The error code associated to these transitions is 3, which corresponds to an uncertainty ranging between 0.001 and 0.01 cm^{-1} (namely, from 30 to 300 MHz);

(b) Line positions calculated using the energy levels reported in reference [11] and retrieved by using the measured active rotational-vibrational energy levels (MARVEL) procedure. We draw the reader's attention on the fact that MARVEL uses high-quality absorption or emission line positions available in the literature to determine and validate the energy levels together with their self-consistent uncertainties. Based on a reweighted inversion process, MARVEL also determines the uncertainty for each energy level. In the case of the (0, 0, 2, 0, 1, 0, 1, e/f)[1] vibrational levels, depending on the particular J-value, the $2-\sigma$ uncertainty ranges from 0.0003 to 0.003 cm^{-1} (namely, from 9 to 90 MHz);

(c) Experimental transition frequencies from the two most recent works based on Fourier transform infrared (FTIR) spectroscopy by Jacquemart *et al* [15] and Lyulin *et al* [16]. For both these studies, the $1-\sigma$ overall uncertainty is 0.001 cm^{-1} (30 MHz).

Figure 4 shows the outcomes of these comparisons. Compared to the data provided by HITRAN, the level of disagreement is well within the error range given in the database, being 26 MHz the root-mean-square (rms) value of the absolute deviations. When our data are compared with those reported in [15], the rms deviation drops to 9 MHz, even though the absolute frequencies differ less than 1 MHz for a few, well isolated, transitions. Only in one case, namely, for the P18e line, the disagreement is larger than the quoted uncertainty of 30 MHz. The comparison becomes more interesting when moving to the data of reference [16]. In fact, the rms deviation is further reduced down to about 3 MHz, the highest deviation being equal to 6.37 MHz, as observed for the P15e transition. The comparison with MARVEL data shows an agreement at the level of about 8 MHz. However, excluding the Q14e transition for which the deviation is 31.51 MHz, the rms deviation decreases to 3.45 MHz, which is comparable to that obtained from the comparison with reference [16]. The discrepancy of the Q14e transition is probably due to the fact that this line is in close proximity (only 177 MHz) to another C_2H_2 strong transition belonging to a different vibrational band. Indeed, among the energy levels reported in [11] and considered in this work, the excited $J = 14$ *para* level is the one having the highest uncertainty, namely, 0.003 cm^{-1}.

[1] $(\nu_1, \nu_2, \nu_3, \nu_4, \nu_5, l_4, l_5, e/f)$ is the normal mode labeling for C_2H_2 vibrational level, indicating e or f the symmetry relative to the Wang transformation. For more details, we refer the reader to [15] or [16].

Table 1. Absolute frequencies of the investigated transitions and comparison to HITRAN [24], MARVEL [11], and to experimental values provided by references [15, 16]. The numbers in parenthesis of the second column represent the $1-\sigma$ statistical uncertainty. Deviations are calculated as present work minus literature values.

Line	Frequency (kHz)	Deviations (MHz)			
	This work	HITRAN [24]	MARVEL [11]	Reference [15]	Reference [16]
P20e	214 866 944 844(13)	0.43	−0.76	−11.56	0.70
P19e	214 949 575 682(10)	−1.72	−0.82	−3.82	−0.82
P18e	215 031 498 086(12)	−25.19	1.49	−31.78	−0.90
P17e	215 112 856 364(7)	66.55	0.87	−1.20	0.57
P16e	215 193 422 757(10)	38.84	−3.70	4.36	−0.20
P15e	215 273 346 202(12)	33.42	5.41	−0.46	6.37
P14e	215 352 613 434(12)	29.83	3.59	−1.05	0.33
P13e	215 431 228 966(2)	26.28	5.06	0.20	2.48
P12e	215 509 198 852(10)	22.25	2.46	−0.23	3.69
Q20e	216 296 117 303(6)	−7.61	4.66	3.19	0.16
Q19e	216 305 817 158(6)	−19.23	1.91	−5.14	1.91
Q17e	216 323 710 523(4)	3.21	4.98	−2.49	5.64
Q16e	216 331 862 772(6)	−12.69	8.66	−10.29	0.65
Q14e	216 346 682 873(5)	−16.12	31.51	1.26	−4.19
Q13e	216 353 347 284(3)	−14.90	1.74	1.59	2.01
Q12e	216 359 518 983(10)	−12.93	−3.79	−0.04	−2.56

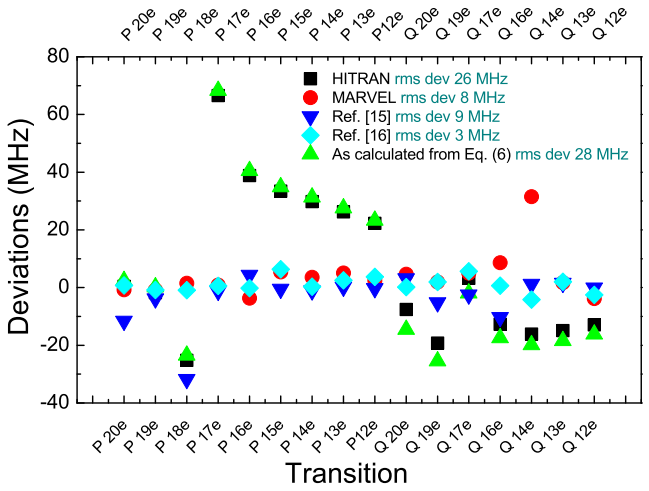

Figure 4. Frequency deviations between the measured line positions and those reported in the HITRAN database [24], those retrieved by the MARVEL procedure [11], those calculated using the isolated band model (equation (6)), and those provided by references [15, 16].

To investigate the reasons for the observed deviations from the HITRAN database, we retrieved the line center frequencies from the energy levels that can be calculated according to the equation:

$$E_{l,h}(J) = G_{l,h} + B_{l,h}J(J+1) - D_{l,h}[J(J+1)]^2 + H_{l,h}[J(J+1)]^3, \quad (6)$$

where $G_{l,h}$ is the vibrational term, $B_{l,h}$, $D_{l,h}$, and $H_{l,h}$ are the rotational and centrifugal constants of the ground (l) and excited (h) vibrational levels, respectively. The values for these constants are taken from table 1 of reference [16]. The deviations of the calculated values from our determinations exhibit a trend that reproduces the one of the HITRAN database, as it is shown in figure 4. Therefore we can conclude that, similarly to the model of equation (6), HITRAN does not take into account the strong vibrational perturbations that affect the excited levels of most of the C_2H_2 bands in the near-infrared [16].

For what concerns the uncertainty of our determinations some further insights must be added. In particular, the whole budget can be quantified according to the entries in table 2. The statistical contribution comes from the weighted linear fit (see figure 3). The OFCS contributes with an uncertainty of 0.5 kHz, which is due to the stability of the GPS-disciplined Rb clock. The uncertainty in the driving frequency of the AOM is estimated to be negligible, being at the Hz-level. Similarly, the contributions originating from the wave front curvature as well as from possible interfering lines can be neglected. Taking into account a root-square mean velocity of about 435 m s^{-1} of the C_2H_2 molecules at 296 K, the

Table 2. Summary of estimated statistical and systematic uncertainties associated to the absolute determination of line center frequencies.

Contribution	Uncertainty	
	Type-A	Type-B
$k = 1$	(kHz)	
Statistical	2–13[a]	
Frequency COMB		0.5
AOM frequency		Negligible
Second-order Doppler effect		0.35
Pressure shift		1.4
Power shift		0.4
Recoil shift		Not present
Interference from neighbor lines		Negligible
Wave front curvature		Negligible
Δ_f[b]		0.225
Total uncertainty	3–13[a]	

[a]Depending on the investigated transition (see table 1).
[b]Δ_f is the contribution due to the difference between the probe laser frequency and the cavity resonance (see section 3 for further details).

second-order Doppler shift is estimated to be 0.35 kHz. As shown by Hall *et al* in reference [32], the recoil shift cancels out in Lamb-dip spectroscopy and, therefore, it is not included in our budget. Varying the intra-cavity power in the range 0.05–0.25 W, we did not observe any influence in the retrieved line center frequencies within the experimental noise. However, adopting a very caution approach, we decide to add a further contribution of 0.4 kHz due to the power shift, according to the outcomes of references [13, 14]. The last component of the uncertainty budget takes into account the frequency difference between the probe (excitation) laser and the cavity resonance, as clearly explained by Reed *et al* [33]. In our experimental conditions, the maximum deviation between the two frequencies amounts to about 1 kHz, for each transient cavity build-up event. Due to the twenty repeated acquisitions of the cavity decay time for each spectral point, nearby the line center, such a deviation should be divided by $(20)^{1/2}$, thus leading to a type-B contribution $\Delta_f = 225$ Hz. Finally, adding in quadrature all the contributions, the $1-\sigma$ uncertainty of the measured line positions varied between 3 and 13 kHz, thus leading to a relative uncertainty of 6×10^{-11} in the worst case. It should be noted that our data give an improvement in the overall uncertainty by more than three orders of magnitude, as compared to the existing data.

4. Test of the MARVEL energies

Line pairs of the P and Q branches are selected so as to form a so-called 'V'-scheme, in which the transitions share the lower energy level. Such a choice made it possible to retrieve the rotational energy separations of the excited vibrational state. We perform these determinations for the rotational levels from 11 to 20 and compared our results with those that can be calculated from the data reported in MARVEL [11], for a stringent test of the algorithm adopted by this method. The results are summarized in table 3. The energy separation of the rotational levels 17–18 and 14–15 could not be determined because we did not record the sub-Doppler features of the Q18e and Q15e lines. Indeed, these C_2H_2 transitions, at 7215.492 690 and 7216.310 220 cm^{-1}, respectively, are very close to strong H_2O absorption lines, circumstance that prevents any reliable acquisition of the Lamb-dip signals.

The level of agreement between our determinations and the MARVEL values is relatively good, better than that expected on the basis of the MARVEL uncertainties. In fact, the absolute deviations that are listed in the fifth column of table 3 are always much smaller than the uncertainties given in [11]. If the energy separations are determined from the transition frequencies reported in HITRAN [24] (data not reported in table 3 for the sake of legibility), it turns out that the deviations are negative, only in one case smaller than 10 MHz (in absolute terms), and with a rms deviation of about 20 MHz, namely, nearly a factor of 2 larger with respect to MARVEL.

Furthermore, looking at table 3, it is not surprising that the highest deviation (27.44 MHz) is found for the 14-13 pair. Indeed, as mentioned above, the MARVEL uncertainty for the $J = 14$ level is particularly poor. Also, it should be noted that the deviations in the case of *para* energy levels are a factor of 5 larger than the *ortho* levels. This is probably due to the fact that *para* transitions exhibit line intensity factors that are about three times smaller than *ortho* lines, and hence, the quality of the experimental data involved in the MARVEL inversion procedure are not as good as that of other lines.

Table 3. Energy separation between selected pairs of rotational levels within the (0, 0, 2, 0, 1, 0, 1, e/f) excited vibrational levels of the C_2H_2 electronic ground state. The numbers in parenthesis of the fourth column represent the uncertainty as calculated from the data of reference [11].

		Energy separation/h[a] (MHz)		
Rotational levels	Nuclear spin	This work	MARVEL [11]	Deviation[b] (MHz)
20-19	*para*	1429172.46	1429 167(72)	5.46
19-18	*ortho*	1356 241.48	1356 239(33)	2.48
17-16	*ortho*	1210 854.16	1210 850(16)	4.16
16-15	*para*	1138 440.02	1138 428(56)	12.02
14-13	*para*	994 069.44	994 042(95)	27.44
13-12	*ortho*	922 118.32	922 122(26)	−3.68
12-11	*para*	850 320.13	850 326(51)	−5.87

[a] h is the Planck constant.
[b] This work minus MARVEL.

5. Conclusions

In conclusion, we recorded for the first time Doppler-free absorption spectra of C_2H_2 in coincidence with sixteen components of the weak $2\nu_3 + \nu_5^1$ vibrational band in the 1.4 μm wavelength region, by using a comb-assisted cavity ring-down spectrometer. We determined the zero-pressure center frequency of the investigated lines with an overall combined standard uncertainty varying between 3 and 13 kHz. These absolute frequencies enabled us to perform a stringent test of the MARVEL procedure for acetylene. More particularly, we could determine the separations for seven pairs of energy levels of the excited vibrational states (0, 0, 2, 0, 1, 0, 1, e/f), for J-values from 11 to 20. Our study provides a validation of the MARVEL procedure. In fact, a satisfactory agreement is found with MARVEL data, the relative deviations being of the order of few parts over 10^6. This is far from the extraordinary agreement (of few parts over 10^8) that we found for the rotational levels of the ground vibrational state of the $H_2^{18}O$ molecule [34]. Therefore, it is confirmed that MARVEL data are less accurate when dealing with excited vibrational levels than with rotational levels. However, deviations of MARVEL from our data are always smaller than MARVEL uncertainties. Our values, if used as further entries of MARVEL, would contribute to a better knowledge of the C_2H_2 energy levels, thus leading to a more accurate line list in the near-infrared. On the other hand, the results of our work confirm the recent findings of reference [35] according to which Doppler-free laser-based experiments, aimed to the accurate determination of the transition frequencies of molecular species, could significantly improve the quality and utility of spectroscopic databases.

Acknowledgments

This research was performed under the program V:ALERE, VAnviteLli pEr la RicErca, call 2019, project V:ANS, funded by Università della Campania 'Luigi Vanvitelli'.

Data availability statement

The data that support the findings of this study are available upon reasonable request from the authors.

ORCID iDs

E Fasci https://orcid.org/0000-0003-1722-5831
S Gravina https://orcid.org/0000-0003-2783-7049
G Porzio https://orcid.org/0000-0002-8398-2649
A Castrillo https://orcid.org/0000-0002-1253-9172
L Gianfrani https://orcid.org/0000-0002-2241-7603

References

[1] Castrillo A, Fasci E, Dinesan H, Gravina S, Moretti L and Gianfrani L 2019 *Phys. Rev. Appl.* **11** 064060
[2] Wagner S, Klein M, Kathrotia T, Riedel U, Kissel T, Dreizler A and Ebert V 2012 *Appl. Phys.* B **107** 585–9
[3] Silvestri F and Marrocchi A 2010 *Int. J. Mol. Sci.* **11** 1471–508
[4] Metsälä M, Schmidt F M, Skyttä M, Vaittinen O and Halonen L 2010 *J. Breath Res.* **4** 046003

[5] Tinetti G et al 2012 Exp. Astron. 34 311–53
[6] Tsiaras A et al 2016 Astrophys. J. 820 99
[7] Rimmer P B et al 2019 Astrophys. J. 888 21
[8] Ridgway S T, Hall D N B, Kleinmann S G, Weinberger D A and Wojslaw R S 1976 Nature 264 345–6
[9] Pascucci I, Herczeg G, Carr J S and Bruderer S 2013 Astrophys. J. 779 178
[10] Chubb K L, Tennyson J and Yurchenko S N 2020 Mon. Not. R. Astron. Soc. 493 1531–45
[11] Chubb K L et al 2018 J. Quant. Spectrosc. Radiat. Transfer 204 42–55
[12] Twagirayezu S, Hall G E and Sears T J 2018 J. Chem. Phys. 149 154308
[13] Di Sarno V, Aiello R, De Rosa M, Ricciardi I, Mosca S, Notariale G, De Natale P, Santamaria L and Maddaloni P 2019 Optica 6 436–41
[14] Tao L-G, Hua T-P, Sun Y R, Wang J, Liu A-W and Hu S-M 2018 J. Quant. Spectrosc. Radiat. Transfer 210 111–5
[15] Jacquemart D, Lacome N, Mandin J-Y, Dana V, Tran H, Gueye F K, Lyulin O M, Perevalov V I and Régalia-Jarlot L 2009 J. Quant. Spectrosc. Radiat. Transfer 110 717–32
[16] Lyulin O M, Vander Auwera J and Campargue A 2015 J. Quant. Spectrosc. Radiat. Transfer 160 85–93
[17] Lyulin O M and Perevalov V I 2017 J. Quant. Spectrosc. Radiat. Transfer 201 94–103
[18] Fasci E, Castrillo A, Dinesan H, Gravina S, Moretti L and Gianfrani L 2018 Phys. Rev. A 98 022516
[19] Fasci E, Dinesan H, Moretti L, Merlone A, Castrillo A and Gianfrani L 2018 Metrologia 55 662–9
[20] Dinesan H, Fasci E, D'Addio A, Castrillo A and Gianfrani L 2015 Opt. Express 23 1757–66
[21] Fasci E, Odintsova T A, Castrillo A, De Vizia M D, Merlone A, Bertiglia F, Moretti L and Gianfrani L 2016 Phys. Rev. A 93 042513
[22] Castrillo A, Fasci E, Galzerano G, Casa G, Laporta P and Gianfrani L 2010 Opt. Express 18 21851–60
[23] Zhang W, Wei H, Chen X and Li Y 2018 Appl. Opt. 57 8487–93
[24] Gordon I et al 2022 J. Quant. Spectrosc. Radiat. Transfer 277 1–82 107949
[25] Ma W, Foltynowicz A and Axner O 2008 J. Opt. Soc. Am. B 25 1144–55
[26] Ma L-S, Ye J, Dubé P and Hall J L 1999 J. Opt. Soc. Am. B 16 2255–68
[27] Giusfredi G, Bartalini S, Borri S, Cancio P, Galli I, Mazzotti D and De Natale P 2010 Phys. Rev. Lett. 104 110801
[28] Wang J, Sun Y R, Tao L-G, Liu A-W, Hua T-P, Meng F and Hu S-M 2017 Rev. Sci. Instrum. 88 043108
[29] Wang J, Sun Y R, Tao L G, Liu A W and Hu S M 2017 J. Chem. Phys. 147 091103
[30] De Vizia M D, Rohart F, Castrillo A, Fasci E, Moretti L and Gianfrani L 2011 Phys. Rev. A 83 052506
[31] Galzerano G, Gambetta A, Fasci E, Castrillo A, Marangoni M, Laporta P and Gianfrani L 2011 Appl. Phys. B 102 725–9
[32] Hall J L, Bordé C J and Uehara K 1976 Phys. Rev. Lett. 37 1339–42
[33] Reed Z D, Long D A, Fleurbaey H and Hodges J T 2020 Optica 7 1209–20
[34] Gambetta A, Fasci E, Castrillo A, Marangoni M, Galzerano G, Casa G, Laporta P and Gianfrani L 2010 New J. Phys. 12 103006
[35] Tóbiás R, Furtenbacher T, Simkó I, Császár A G, Diouf M L, Cozijn F M J, Staa J M A, Salumbides E J and Ubachs W 2020 Nat. Commun. 11 1708